LOW-TEMPERATURE CREEP OF BITUMINOUS COMPOSITES: NEW INSIGHTS FROM BENDING-BEAM EXPERIMENTS

Roman Lackner[1], Markus Spiegl[2], Ronald Blab[2], and Josef Eberhardsteiner[1]

Christian Doppler Laboratory on "Performance-based Optimization of Flexible Road Pavements"

[1]Institute for Strength of Materials, Vienna University of Technology, Karlsplatz 13/202, 1040 Vienna, Austria
[2]Institute for Road Construction and Maintenance, Vienna University of Technology, Gußhausstraße 28/233, 1040 Vienna, Austria

ABSTRACT

This paper deals with upscaling of creep parameters of bitumen-filler composites (mastic) within the framework of a multiscale model for asphalt. Restricting the present study to low-temperature creep, bending-beam creep tests at temperatures below 0 °C are performed. Based on the obtained experimental results, parameters describing low-temperature creep of *pure* bitumen are identified. The filler is considered as rigid inclusion embedded into a viscous matrix within the framework of continuum micromechanics. The creep parameters for the mastic, obtained from the application of appropriate homogenization schemes, are validated by additional bending-beam experiments. The good agreement between experimental results and model prediction shows that the filler affects the creep parameters only by its volume fraction, entering the proposed multiscale model.

1. INTRODUCTION

Low-temperature creep of asphalt provides the stress relaxation capacity in flexible pavements required to avoid cracking as consequence of thermal shrinkage during cold winter periods. The viscosity of asphalt and, hence, its creep capacity is mainly linked to the rheological behaviour of the employed binder material, the bitumen. In order to develop a material model applicable to the wide range of asphalt mix types commonly used for pavement construction, the multiscale approach, comprising five scales of observation, is chosen (see Fig. 1).

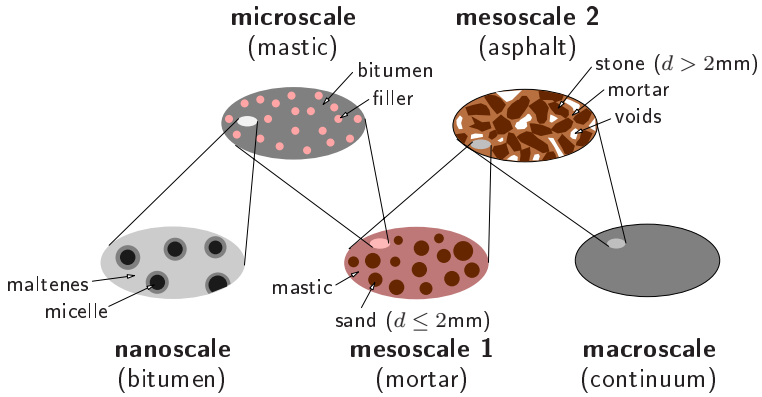

Fig. 1. Multiscale model for asphalt comprising five scales of observation.

Hereby, at the lowest (*bitumen*-) scale, with a characteristic length of a few µm, the material is composed of clusters of large-scale molecules (asphaltenes) distributed in the maltene matrix [1,10]. At the next higher scale, the so-called *mastic*-scale, the filler, i.e., aggregates with a diameter lower than 125 µm, is introduced. The input data for multiscale models, such as shown in Figure 1, are the mechanical properties, the volume fractions, and the shape of the constituents and the interaction between different constituents (asphaltenes, maltenes, filler, …). By means of upscaling of information from one to the next higher scale of observation it is aimed to finally obtain macroscopic material parameters for macroscopic analyses of flexible pavements. Multiscale models, once having established an appropriate upscaling scheme, are applicable to different asphalt mixes, to asphalts consisting of different constituents as well as to asphalts undergoing chemomechanical changes of one or more

constituents, resulting from environmental influences. As regards the latter, such changes can be considered at the respective scale of observation (e.g., oxidation of bitumen at the *bitumen*-scale), providing – via upscaling – the effect of these changes on the macroscopic material response.

In this paper, an upscaling procedure for parameters describing low-temperature creep of the bitumen-filler composite at the *mastic*-scale is presented. The experimental basis is provided by bending-beam experiments, conducted for different types of bitumen and filler. In the following section, the considered types of bitumen and filler are briefly described and basic information regarding the employed experimental setup is provided. Thereafter, results from bending-beam experiments of *pure* bitumen are presented, allowing to identify parameters describing low-temperature creep of bitumen. Then, the micromechanical model for the bitumen-filler composite is described, using the identified parameters for *pure* bitumen as input. Finally, the performance of the micromechanical model, providing estimates for the creep parameters for the bitumen-filler composite, is validated by additional bending-beam experiments.

2. MATERIALS & METHODS

In order to cover a wide range of different bitumen-filler combinations, five types of bitumen, ranging from very soft to air-blown (very hard) bitumen (see Table 1), and four types of filler were considered in the experimental program (see Table 2).

Table 1. Characteristics of bitumens considered in the experimental program (bitumen notation acc. to [11]).

type of bitumen	characterization	penetration depth [1/10 mm]	breaking point [°C]	softening point [°C]
B90/10	hard (air-blown) bitumen	7	4	87
B50/70	standard bitumen	49	-13	51
B70/100	standard bitumen	72	-17	47
B160/220	soft bitumen	151	-17	40
pmB60/90	SBS polymer-modified bitumen	64	-18	58

Table 2. Properties of fillers considered in the experimental program.

type of filler	mineralogy	real mass density ρ_f [kg/m³]	air voids f_a [vol-%]	surface [m²/kg]
hydrated lime	lime	2230	64.0	15800
limestone dust	calcite, dolomite	2710	30.5	2050
Magyer	quartz, dolomite, calcite, mica, feldspar	2760	35.2	4990
Schremser granite	mica, quartz, feldspar	2700	37.1	2580

The fillers vary in the specific surface, mineralogy (acid or alkaline), grain shape, and grading curve (see Fig. 2). Following the multiscale concept mentioned in the introduction, experiments for the identification of filler properties were conducted, providing (i) the real mass density ρ_f (pycnometer), (ii) the air voids f_a (Ridgen test [9]), and (iii) the specific surface (BET method [12]).

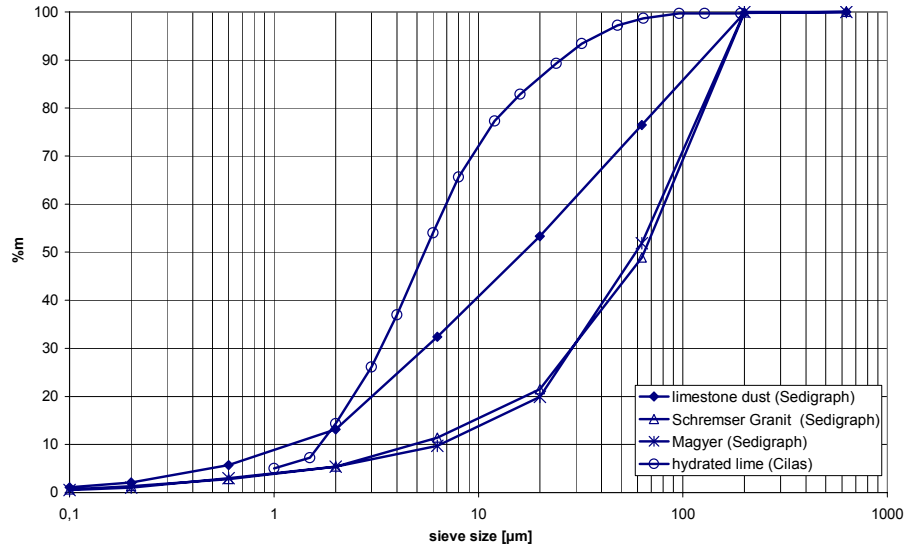

Fig. 2. Grading curve of fillers considered in the experimental program.

For the identification of creep parameters of *pure* bitumen, on the one hand, and for the validation of the micromechanical model for the bitumen-filler composite, on the other hand, bending-beam experiments were performed. The employed bending-beam rheometer (BBR) is a three-point bending-beam test, designed to characterize the low-temperature behaviour of bituminous binders. Hereby, a beam-shaped specimen with the dimensions 125 x 12.5 x 6.25 mm is placed horizontally on two bearings (spacing l = 102 mm) which are submerged into an ethyl alcohol bath, providing a constant, pre-specified temperature. In standard BBR testing, a load F of 980 mN is applied for four minutes at the mid-span of the beam (see Fig. 3).

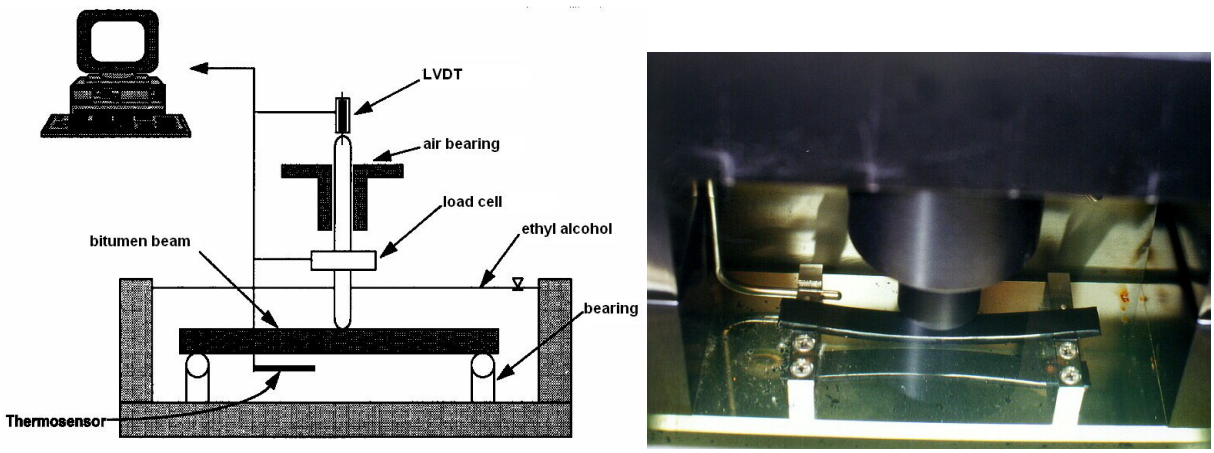

Fig. 3. BBR: experimental setup [2]

Commonly, the creep stiffness S is computed from the monitored displacement history $u(t)$, using linear-elastic beam theory, as

$$S(t) = \frac{Fl^3}{4u(t)bh^3}, \tag{1}$$

where b, h, and l refer to the width, height, and the length of the beam. In addition to the creep stiffness, a so-called m-value, referred to as the logarithmic creep rate, is determined. The m-value represents the slope of tangent to log S – log t graph at t = 60 s (see Fig. 4).

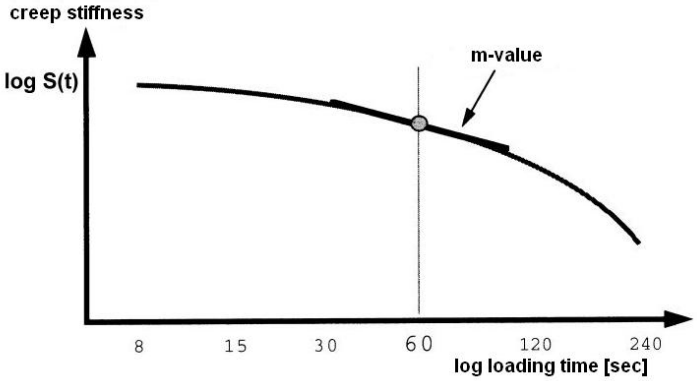

Fig. 4. BBR: definition of the *m*-value [3].

The extension of formulas derived from beam theory based on linear-elastic material response to viscoelastic material behaviour, as done in Equation (1), is only valid if both the strain and stress distribution over the cross-section of the beam remains linear. This, on the other hand, implies that the evolution of the creep strain depends linearly on the applied stress. In order to validate this assumed linearity, BBR tests characterized by three different load levels were performed. In addition to the standard load of 980 mN, a load of 490 and 1960 mN were considered. Figure 5 shows the measured displacement after four minutes, normalized by the applied load F, as a function of F. The obtained results clearly indicate the linearity of the underlying creep behaviour, with $u/F \propto$ constant and, hence, $u \propto$ constant $\times F$.

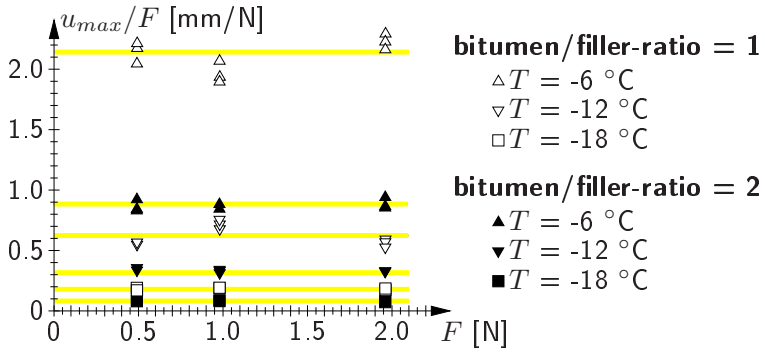

Fig. 5. Maximum deflection obtained from BBR experiments after four minutes of loading considering different load levels (B70/100, limestone-dust filler, bitumen/filler-ratio in [mass-%]).

In case of a linear-elastic material behaviour, the stress at the bottom fibre of the mid-span cross-section and the respective deflection of this cross section are given by

$$\sigma = \frac{Fl/4}{bh^2/6} \qquad \text{and} \qquad u = \frac{Fl^3}{48EI}. \tag{2}$$

Considering Equations (2) in $\varepsilon = \sigma / E$ gives the strain in the bottom fibre as a function of the measured displacement, reading $\varepsilon = 6hu/l^2$. Finally, the compliance J [MPa^{-1}] is obtained in the form

$$J = \frac{\varepsilon}{\sigma} = \frac{4bh^3}{Fl^3} u \ \text{[MPa}^{-1}\text{]}. \tag{3}$$

In case of linear creep, Equation (3) can be applied to the displacement history measured during BBR-tests, yielding the compliance J as a function of time, with $J(t) \propto u(t)$. In the remaining part of the paper, the creep compliance J [MPa^{-1}] and the creep-compliance rate dJ/dt [MPa^{-1}s^{-1}] will be used instead of the commonly employed parameter S and the m-value.

3. LOW-TEMPERATURE CREEP OF BITUMEN

In order to avoid the interpretation of experimental results on the basis of the empirical parameters *S* and *m* [3], rheological models were employed to identify creep characteristics from bending-beam experiments, such as e.g. Burger's model, as reported in [4]. The creep compliance of Burger's model for a testing time of four minutes is illustrated in 6(a). While the creep compliance of Burger's model approaches a line with a slope defined by the single dash-pot, long-term BBR tests, characterized by extending the loading time to one hour, revealed a continuous decrease of the compliance rate. This discrepancy between the experimental results and the approximation by Burger's model is illustrated in 6(b).

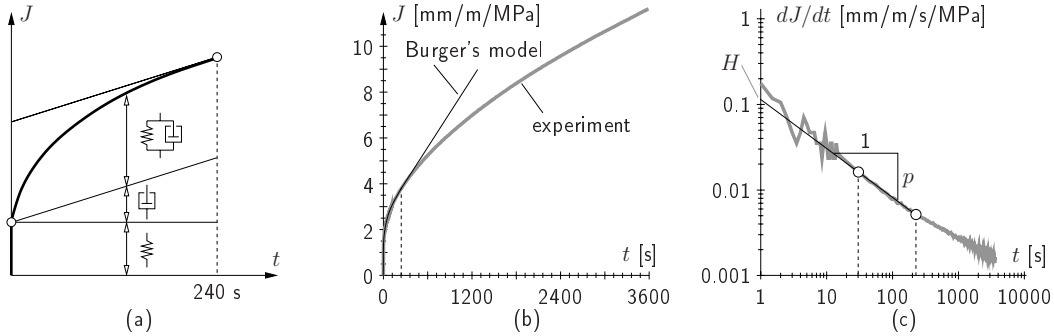

Fig. 6. Creep compliance of Burger's model: (a) different contributions to compliance and (b) comparison with experimental data; (c) experimental result for creep-compliance rate *dJ/dt* (B70/100, F = 980 mN, T = -18 °C).

As a remedy, the identification of parameters with a clear physical background is proposed in this paper. For this purpose, the creep compliance rate *dJ/dt*, commonly plotted in the log *dJ/dt* - log *t* diagram (see Fig. 6(c)), is approximated by a linear function, reading

$$dJ/dt \approx Ht^p, \tag{4}$$

giving the creep compliance as $J(t) \approx J_0 + H(p+1)t^{p+1}$. In Equation (4), H [MPa^{-1}s^{-1}] represents the creep compliance rate at t = 1 s and p [-] is the slope of the linear approximation function in the log *dJ/dt* - log *t* diagram, with $p < 0$. In the following, the parameters H and p are obtained from a least-square minimization problem, aiming at best possible match between the experimental results and the approximation function Ht^p within the time interval $30 < t < 230$ s.

Figure 7 shows the values for H and p determined from standard BBR results of the bitumens considered in this study. The increase of p with increasing temperature is related to changes in the bitumen microstructure. This microstructure is characterized by the co-existence of parts in both the glassy and the viscous (rubber-like) state, resulting from the molecular cocktail in bitumen, comprising saturates, aromates, resins, and asphaltenes. Moreover, the large-size, polar molecules (resins and asphaltenes) aggregate to string-like structures ("bee-shaped" structures, see [6]). Whereas these "bee-shaped" structures seem to remain within the considered temperature range from -24 to 0°C, the glassy part in bitumen composed resins, aromates, and saturates, decreases with increasing temperature and, hence, the creep capacity increases. This is reflected by the increase of p with increasing temperature. Based on the experimental results, *p(T)* may be approximated by a linear function, reading (see Fig. 7(b))

$$p(T) = p_0 + c\left(T - \overline{T}\right) \quad \text{(with } T \text{ in [°C] and } \overline{T} = \text{-12 °C)}, \tag{5}$$

where p_0 [-] and c [°C^{-1}] are constant parameters, which need to be specified for the different types of bitumen. In case of B70/100, p_0 = -0.42 and c = 0.01 °C^{-1} (see Fig. 7(b)). Whereas the change of the slope of the compliance rate is associated with changes in the microstructure of bitumen, the increase of the compliance, represented by the value of H, with increasing

temperature is related to increased mobility of the molecules. This increase of mobility is accounted for by an Arrhenius-type law, reading

$$H = H_0 \exp\left[-\frac{E_a}{R}\left(\frac{1}{T} - \frac{1}{\overline{T}}\right)\right] \quad \text{(with } T \text{ in [K] and } \overline{T} = 261 \text{ K)}, \tag{6}$$

or, respectively,

$$\ln H = \left(\ln H_0 + \frac{E_a}{R\overline{T}}\right) - \left(\frac{E_a}{R}\right)\frac{1}{T} \quad \text{(see Fig. 7)}, \tag{7}$$

where in a first approximation H_0 [MPa^{-1}] and the activation energy E_a [J/MOL] are assumed to be constant. For B70/100, these parameters were identified as H_0 = 0.0004 MPa^{-1}s^{-1} and E_a/R = 9000 K (see Fig. 7(a)), where R is the gas constant, with 8.31 J/MOL/K. In fact, the identified parameters p_0, c, H_0, and E_a, describing low-temperature creep of bitumen, depend on the molecular composition of the considered bitumen and should be related to the glassy – viscous (rubber-like) state. Within the multiscale model, this dependency is addressed at the *bitumen*-scale which is not the focus of *this* paper. In the following, Equations (5) and (6) with the parameters given for B70/100 will be used to describe low-temperature creep of the bitumen *phase*.

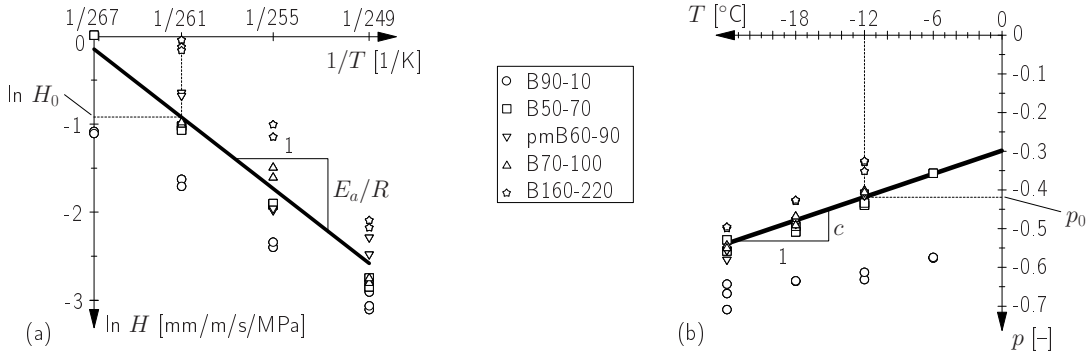

Fig. 7. H and p determined for different types of bitumen at different temperatures: (a) identification of Arrhenius law describing the temperature dependence of H and (b) linear relation between p and T.

4. FILLER-BITUMEN INTERACTION – THE MICROMECHANICAL MODEL

The micromechanical model for the bitumen-filler composite is formulated within the framework of continuum micromechanics. Following the three-step procedure of continuum micromechanics, the following subsections deal with (i) the representation, (ii) the localization, and (iii) the homogenization of the bitumen-filler composite.

4.1. Representation

The representation of a material comprises the definition of homogeneous constituents (material phases) as well as their assemblages. For the determination of macroscopic material properties of asphalt, five scales of observation are considered in the representation of the material (see Fig. 1), requiring scale transition from the *bitumen*-scale to the *macro*scale. This paper concentrates on the interaction between bitumen and filler at the *mastic*-scale. The length of the representative volume element (RVE) of the *mastic*-scale must be both considerably larger than the filler dimensions and considerably smaller than the size of the RVE representing the next higher scale, the *mortar*-scale. Accordingly, the RVE of the *mastic*-scale has the size of approximately 1 mm and consists of inclusions (filler particles) embedded in the bitumen matrix (two-phase system, see Fig. 8).

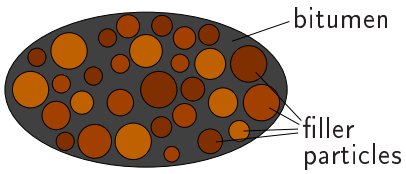

Fig. 8. Micromechanical model: representative volume element (RVE) for bitumen-filler composite (matrix-inclusion morphology; matrix: bitumen; inclusions: filler particles).

As regards the creep properties of the constituents at the *mastic*-scale, viscous deformations in the filler phase are assumed to be zero. This assumption is reasonable, since under the range of loading considered in the present study, the filler exhibits only elastic material response. The viscous behaviour of bitumen, on the other hand, is described by the creep parameters H and p identified in the previous section.

4.2. Localization & homogenization

The local strain tensor in the bitumen and filler phases, $\underline{\underline{\varepsilon}}_b$ and $\underline{\underline{\varepsilon}}_f$, are related to the homogeneous strain tensor $\underline{\underline{E}}$ by the so-called localization tensor $\underline{\underline{\underline{\underline{A}}}}$, reading

$$\underline{\underline{\varepsilon}}_b(\underline{x}) = \underline{\underline{\underline{\underline{A}}}}_b(\underline{x}) : \underline{\underline{E}} \quad \text{and} \quad \underline{\underline{\varepsilon}}_f(\underline{x}) = \underline{\underline{\underline{\underline{A}}}}_f(\underline{x}) : \underline{\underline{E}}. \tag{8}$$

The homogenized stiffness tensor $\underline{\underline{\underline{\underline{C}}}}$ is obtained by the introduction of constitutive relations for the different phases, with $\underline{\underline{\underline{\underline{c}}}}$ as the local phase stiffness tensor, reading

$$\underline{\underline{\Sigma}} = \left\langle \underline{\underline{\sigma}} \right\rangle_V = \left\langle \underline{\underline{\underline{\underline{c}}}} : \underline{\underline{\varepsilon}} \right\rangle_V = \left\langle \underline{\underline{\underline{\underline{c}}}} : \underline{\underline{\underline{\underline{A}}}} \right\rangle_V : \underline{\underline{E}} \equiv \underline{\underline{\underline{\underline{C}}}} : \underline{\underline{E}} \quad \Rightarrow \quad \underline{\underline{\underline{\underline{C}}}} = \left\langle \underline{\underline{\underline{\underline{c}}}} : \underline{\underline{\underline{\underline{A}}}} \right\rangle_V, \tag{9}$$

where $\langle \bullet \rangle_V = 1/V \int_V \bullet \, dV$ is the volume average and $\underline{\underline{\Sigma}}$ represents the homogeneous stress tensor. An estimate for the homogenized stiffness tensor follows from Equation (9), reading

$$\underline{\underline{\underline{\underline{C}}}}^{est} = f_b \underline{\underline{\underline{\underline{c}}}}_b : \underline{\underline{\underline{\underline{A}}}}_b^{est} + f_f \underline{\underline{\underline{\underline{c}}}}_f : \underline{\underline{\underline{\underline{A}}}}_f^{est}, \tag{10}$$

where f_r, $\underline{\underline{\underline{\underline{c}}}}_r$, and $\underline{\underline{\underline{\underline{A}}}}_r^{est}$ denote the volume fraction, the stiffness, and the estimate for the localization tensor of the r-th phase. In case of an inclusion-matrix morphology as depicted in Figure 8, the estimate for the yet unknown localization tensor is provided by the Mori-Tanaka (MT) scheme [5] as

$$\underline{\underline{\underline{\underline{A}}}}_{f(MT)}^{est} = \left[\underline{\underline{\underline{\underline{1}}}} + \underline{\underline{\underline{\underline{S}}}}_f : \left(\underline{\underline{\underline{\underline{c}}}}_b : \underline{\underline{\underline{\underline{c}}}}_f - \underline{\underline{\underline{\underline{1}}}} \right) \right]^{-1} : \left\langle \left[\underline{\underline{\underline{\underline{1}}}} + \underline{\underline{\underline{\underline{S}}}}_f : \left(\underline{\underline{\underline{\underline{c}}}}_b : \underline{\underline{\underline{\underline{c}}}}_f - \underline{\underline{\underline{\underline{1}}}} \right) \right]^{-1} \right\rangle_V^{-1}, \tag{11}$$

where $\underline{\underline{\underline{\underline{S}}}}_f$ is the Eshelby tensor of the filler phase. The respective localization tensor for the bitumen matrix is obtained from $\underline{\underline{\underline{\underline{A}}}}_{f(MT)}^{est}$ and $f_b \underline{\underline{\underline{\underline{A}}}}_b^{est} + f_f \underline{\underline{\underline{\underline{A}}}}_f^{est} = \underline{\underline{\underline{\underline{1}}}}$. In case of spherical, rigid inclusions embedded into an incompressible matrix, Equation (10) can be simplified to an expression for the homogenized shear modulus (see, e.g., [7]), reading

$$\mu_{(MT)}^{est} = \mu_b \left(1 + \frac{5}{2} \frac{f_f}{1 - f_f} \right), \tag{12}$$

while the bulk modulus k^{est} becomes ∞. In Equation (12), the volume fraction of the filler, f_f [-], is determined from the volume of bitumen and filler, V_b [m^3] and V_f [m^3], reading

$$f_f = \frac{V_f}{V_b + V_f} = \frac{m_f / \rho_f}{m_b / \rho_b + m_f / \rho_f} = \frac{(m_f / m_b) / \rho_f}{1 / \rho_b + (m_f / m_b) / \rho_f}, \tag{13}$$

where commonly the ratio between the filler mass m_f and the bitumen mass m_b, m_f/m_b-ratio, is specified in BBR experiments. In Equation (13), ρ_f is given in Table 2 and the density of bitumen ρ_b = 1030 kg/m^3.

Based on the estimate for the shear stiffness of the homogenized material given in Equation (12), the creep parameter H, representing the compliance of the homogenized material, is estimated from

$$H_{(MT)}^{est} = H_b(H_0, T) \times \left(1 + \frac{5}{2} \frac{f_f}{1 - f_f}\right)^{-1}, \tag{14}$$

where H_b represents the creep parameter H for the bitumen matrix, available from Equation (6).

4.3. Validation of micromechanical model

Equation (14) is used for the estimation of the creep parameter H for different bitumen-filler composites made of B70/100 and the fillers listed in Table 2. The values for H predicted by the micromechanical model are shown in Figure 9.

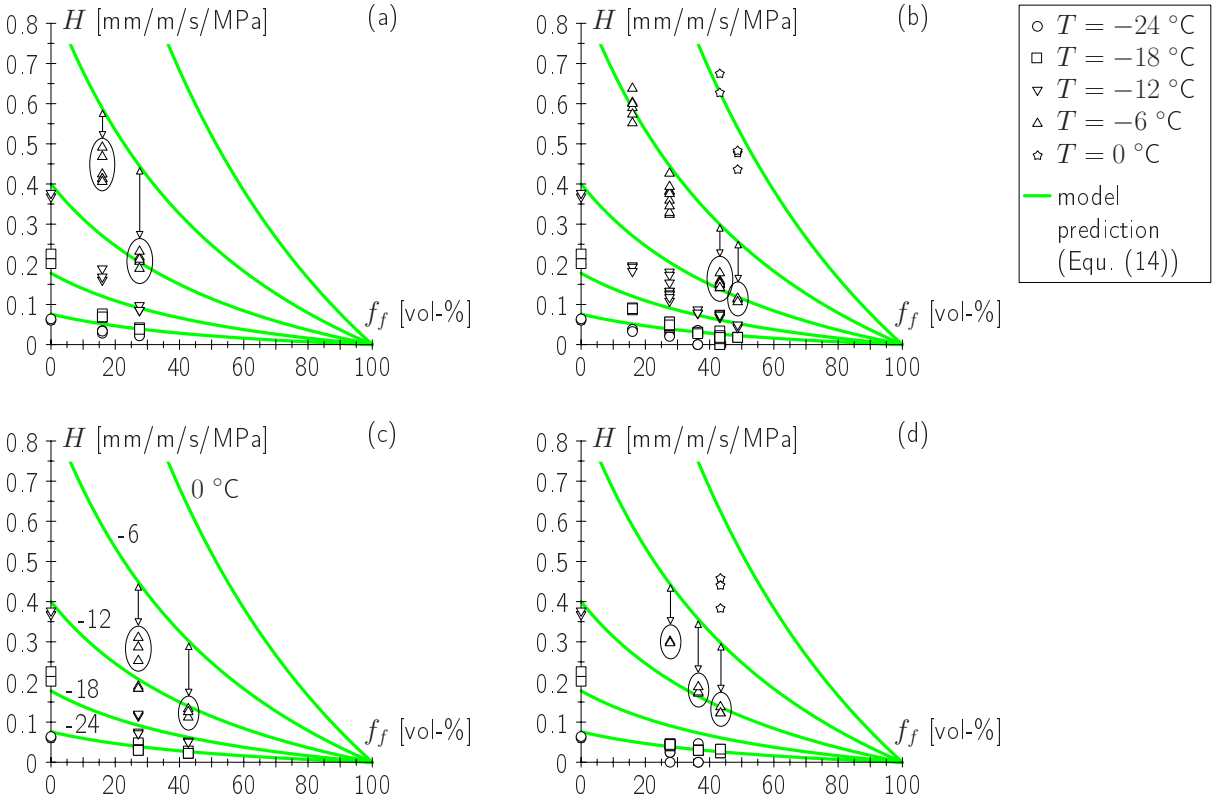

Fig. 9. Validation of micromechanical model for mastic consisting of B70/100 and (a) hydrated-lime, (b) limestone-dust, (c) Magyer, and (d) Schremser filler (used parameters: H_0 = 0.4 mm/m/s/MPa, E_a/R = 9000 K).

The prediction of the creep parameter H by Equation (14) results in a significant overestimation of the respective experimental data. For all types of filler, in Figure 9 this is indicated for the results corresponding to T = -6°C. However, a similar situation is observed

for the other experimental results obtained from different testing temperatures. For bending-beam experiments characterized a creep parameter H exceeding 0.4 mm/m/s/MPa (see testing temperature of 0°C), the compliance of the tested bitumen-filler composite was too large, resulting in deflections of the bending beam reaching 4 mm. However, the geometrical effects in consequence of a deflection/span-ratio of $4/102 \approx 1/25$ are not captured by Equations (2) and (3), which were derived for the geometrically-linear situation.

As a remedy for the observed overestimation of H by the micromechanical model, the consideration of the *effective* volume content of the filler is proposed (see, e.g., [8]). The *effective* volume of the filler is obtained as the sum of the volume of the filler particles and the volume of the air voids f_a in case of full filler compaction that is determined from the Ridgen experiment [9] (see Table 2). The packing volume V_p is obtained from f_a as

$$V_p = \frac{1}{1-f_a}. \tag{15}$$

Replacing f_f in Equation (14) by the *effective* filler content $V_p f_f$, with $V_p f_f > f_f$, yields

$$H_{(MT)}^{est} = H_b(H_0, T) \times \left(1 + \frac{5}{2} \times \frac{V_p f_f}{1 - V_p f_f}\right)^{-1}. \tag{16}$$

Consideration of the *effective* filler content within the micromechanical model results in a good agreement between the experimentally-obtained values for H and the model prediction (see Figure 10). The deviations observed in Figures 10(b) and (d) is explained by the large compliance of the mastic at a testing temperature of 0 °C. The underestimation of H in Figure 10(a) for T = -6 °C, on the other hand, is explained by the consistency and high viscosity of mastic containing hydrated-lime filler (especially for filler volume fractions exceeding 25%), resulting from the large specific surface of hydrated lime (see Table 2).

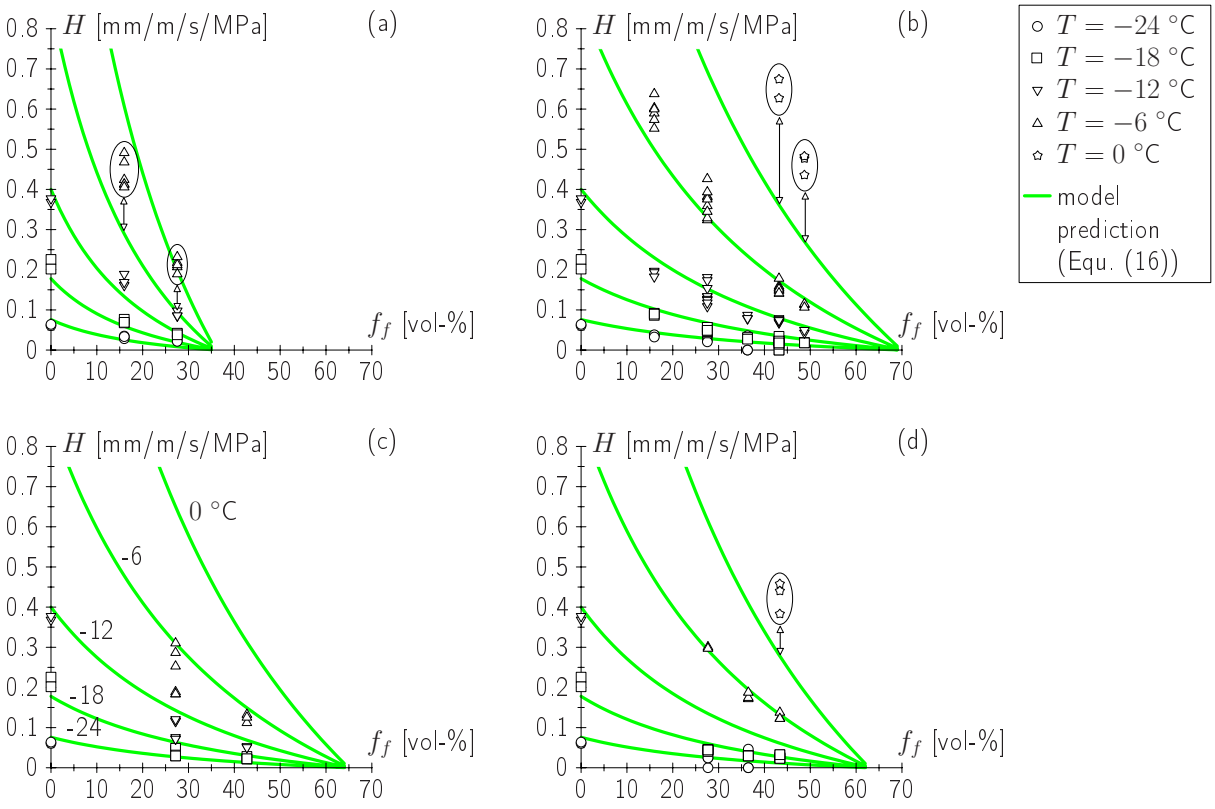

Fig. 10. Validation of micromechanical model for mastic consisting of B70/100 and (a) hydrated-lime, (b) limestone-dust, (c) Magyer, and (d) Schremser filler employing the *effective* volume concept (used parameters: H_0 = 0.4 mm/m/s/MPa, E_a/R = 9000 K).

In addition to the creep parameter H, the influence of the amount of filler on the slope p of the linear approximation function in the log dJ/dt - log t diagram is investigated. Figure 11 shows the experimentally-obtained values for p for mastic consisting of B70/100 and the fillers listed in Table 2 as well as the result of Equation (5), assuming a linear relation between p and T, with p_0 = -0.42 and c = 0.01 °C^{-1}. Although a slight decrease of p is observed for increasing filler content, the value of p seems to be determined by the behaviour of the used bitumen. All values for p are found in the range from -0.60 to -0.25, independent of the type of filler.

Finally, the prediction of the creep parameters H and p by the proposed micromechanical model is assessed for all considered types of bitumen and fillers (see Tables 1 and 2). For this purpose, the parameters of *pure* bitumen H_0, E_a/R, and p_0, and c, already identified for B70/100, are determined for the remaining types of bitumen (see Table 3).

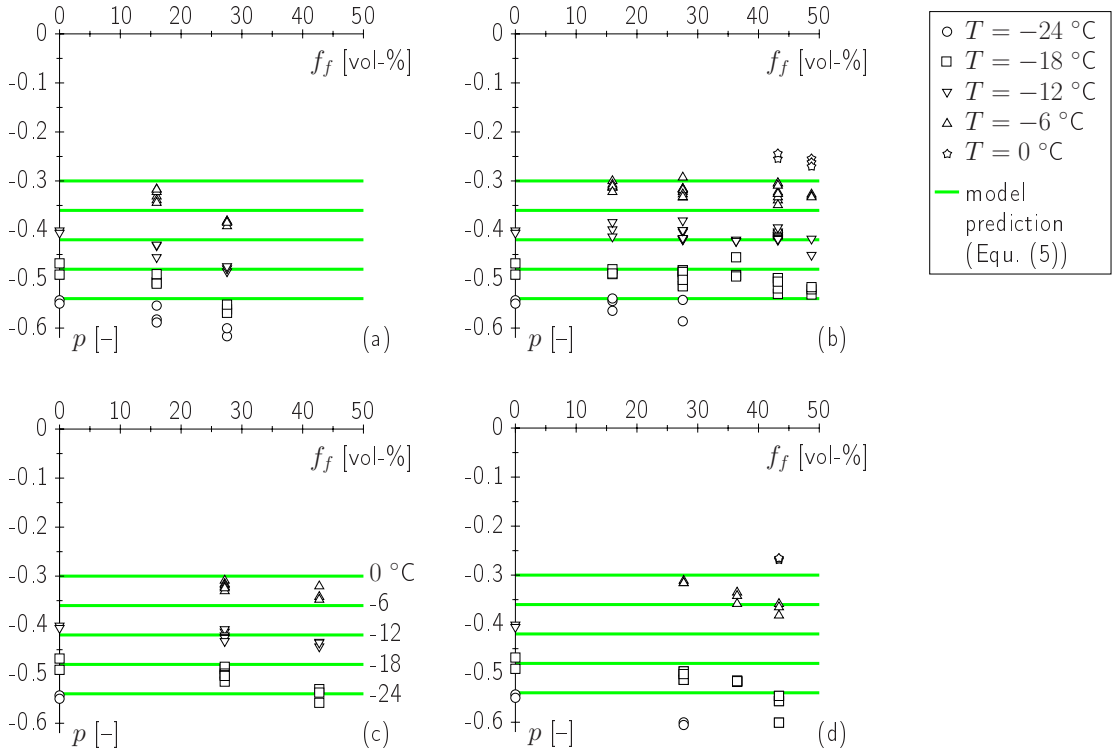

Fig. 11. Predicted and measured creep parameter p for mastic consisting of B70/100 and (a) hydrated-line, (b) limestone-dust, (c) Magyer, and (d) Schremser filler (used parameters: p_0 = -0.42, c = 0.01 °C^{-1}).

Table 3. Parameters describing low-temperature creep of the *(pure)* bitumens considered in the experimental program.

type of bitumen	H_0 [mm/m/s/MPa]	E_a/R [K]	p_0 [-]	c [°C^{-1}]
B90/10	0.21	9000	-0.60	0.01
B50/70	0.34		-0.44	
B70/100	0.40		-0.42	
pmB60/90	0.51		-0.42	
B160/220	0.71		-0.36	

Remarkably, since E_a/R and c are assumed to be constant for all types of bitumen, low-temperature creep is fully described by only two parameters, namely H_0 and p_0 (see Table 3). The obtained results are plotted in Figure 12, showing an excellent agreement between the experimental data and the prediction by the micromechanical model. As already observed in Figure 10, geometrical effects in case of large deflections of the bending beam cause an increase of the deflection and, hence, a shift of the value for the parameter H (see Fig. 12(a)).

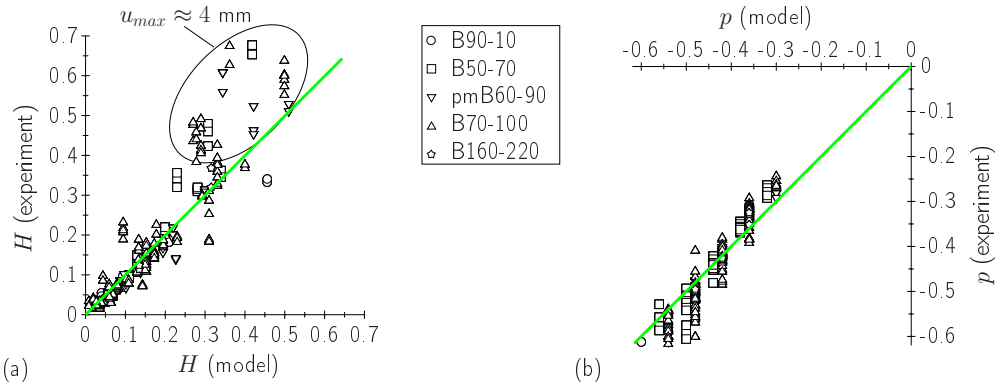

Fig. 12. Comparison between experimental results for creep parameters (a) H [mm/m/s/MPa] and (b) p [-] and the prediction by the micromechanical model via Equations (16) and (5) (all types of bitumens and all types of fillers included → 306 BBR experiments).

5. CONCLUSIONS & OUTLOOK ON FUTURE WORK

In this paper, first results of a multiscale model for asphalt, focusing on low-temperature creep of the bitumen-filler composite, were presented. After identification of two creep parameters describing the viscous behaviour of *pure* bitumen, a micromechanical model, allowing the extension of the description of low-temperature creep towards bitumen-filler composites, was proposed. From the comparison between the creep parameters estimated by the micromechanical model and the respective experimental results, the following conclusions can be drawn:

- Since the filler is considered as rigid inclusion within the micromechanical model, the good agreement between model prediction and experimental results indicates that the filler affects low-temperature creep in form of rigid obstacles randomly distributed within the viscous bitumen matrix.

- So far, the filler was represented by spherical inclusions, disregarding the actual shape of the filler particles. Accordingly, only the volume fraction, which was considered within the micromechanical model, seems to affect the creep properties of the bitumen-filler composite. Whereas the extension of the micromechanical model to ellipsoidal particles is straightforward (the employed Mori-Tanaka scheme was originally developed for ellipsoidal inclusions), the determination of the actual average shape of the filler particles is a topic of ongoing research.

- While the filler significantly affected the amount of the initial value of the creep compliance (parameter H), it had only marginal effect on the reduction of dJ/dt with time, described by the parameter p. The latter was mainly affected by the type of the used bitumen rather than of the type and the amount of filler.

While this paper focused only on homogenization at the *mastic*-scale, providing material information for the next higher, the *mortar*-scale, future work will be devoted to the improvement and extension of the anticipated multiscale model. On the one hand, the creep parameters for *pure* bitumen used in this paper may be related to properties at the *bitumen*-scale (chemical composition of bitumen and microstructure). First research results on this topic are reported in [6]. On the other hand, upscaling of material properties towards the *macro*scale provides macroscopic material properties, serving as input for macroscopic analyses of flexible road pavements.

ACKNOWLEDGEMENTS

The authors thank Babara Gagliano, Andreas Jäger, Karl Kappl, and Michael Wistuba from the Christian Doppler Laboratory on "Performance-based Optimization of Flexible Road Pavements" for fruitful discussions and helpful comments. The authors are indebted to Martin Hopfgartner, Thomas Riedmayer, Johann Schuch, and Roman Slany for the conduction of the bending-beam experiments. Financial support by the Christian Doppler Forschungsgesellschaft (Vienna, Austria) is gratefully acknowledged.

References

1. **Shell-Bitumen UK (1990):** ***The Shell Bitumen Handbook*****. Shell UK, volume 1, Chertsey.**

2. **Cannon Instrument Company (1998):** ***Cannon Bending-Beam Rheometer with Software for Windows 95 and NT - Instruction & Operation Manual for BBR and TE-BBR Models*****. Version 1.1a, August 1998.**

3. **SHRP -- Strategic Highway Research Program (1994):** ***Binder Characterization and Evaluation. Volume 4: Test Methods (SHRP-A-370)*****. National Research Council, Washington DC.**

4. **L.S. Johansson and U. Isacsson (1998):** ***Effect of Filler on Low Temperature Physical Hardening of Bitumen*****. Construction and Building Materials, 12: 463-470.**

5. **T. Mori and K. Tanaka (1973):** ***Average Stress in Matrix and Average Elastic Energy of Materials with Misfitting Inclusions*****. Acta Metallurgica, 21: 571-574.**

6. **A. Jäger, R. Lackner, Ch. Eisenmenger-Sittner, R. Blab (2004):** ***Identification of four material phases in bitumen by atomic force microscopy*****. International Journal of Road Materials and Pavement Design. Accepted for publication.**

7. **D. Gross and Th. Seelig (2001):** ***Bruchmechanik [Fracture mechanics]*****. Springer, Berlin. In German.**

8. **J.W. Ewers and W. Heukelom (1964):** ***Die Erhöhung der Viskosität von Bitumen durch die Zugabe von Füller*****. Straße und Autobahn, 2: 31-39. In German.**

9. **P.J. Ridgen (1954):** ***The Rheology of Non-Aqueous Suspensions*****. Road Research Technical Papers N.S. 28, London.**

10. **A. Jäger (2004):** ***Microstructural identification of bitumen by means of atomic force microscopy (AFM), modulated differential scanning calorimetry (MDSC), and reflected light microscopy (RLM)*****. Master's thesis. Vienna University of Technology, Vienna.**

11. **EN 12591 (1999).** ***Bitumen and bituminous binders – Specifications for paving grade bitumens*****.**

12. **S. Brunauer, P.H. Emmett, E. Teller (1938).** ***Adsorption of gases in multimolecular layers*****. Journal of the American Chemical Society, 60: 309-319.**